Comparative Analysis of Turbulence Models for Automotive Aerodynamic Simulation and Design

Article *in* International Journal of Automotive Technology · April 2019

DOI: 10.1007/s12239-019-0107-7

International Journal of Automotive Technology, Vol. 20, No. 6, pp. 1145–1152 (2019)
DOI 10.1007/s12239–019–0107–7

pISSN 1229–9138/ eISSN 1976–3832

COMPARATIVE ANALYSIS OF TURBULENCE MODELS FOR AUTOMOTIVE AERODYNAMIC SIMULATION AND DESIGN

Dastan Igali, Olzhas Mukhmetov, Yong Zhao*, Sai Cheong Fok and Soo Lee Teh

Department of Mechanical Engineering, School of Engineering, Nazarbayev University, Astana 010000, Kazakhstan

(Received 10 May 2018; Revised 26 February 2019; Accepted 4 April 2019)

ABSTRACT–The reduction of energy consumption and environmental impacts of road vehicles is always a major design objective. Many investigations suggest that reducing aerodynamic drags such as pressure drag and skin friction drag is a more efficient method than engine modification in achieving the design objective. Turbulent flow around a bluff body is notoriously difficult to simulate accurately due to the complexity of the flow conditions around the body, such as complex flow separation and laminar to turbulent flow transition. This paper investigates the flow over a benchmark model called the Ahmed body with a slant angle of 25°, which is considered a challenging problem for RANS approach with two-equation turbulence models (Menter, 1994; Serre *et al*., 2013). Three popular turbulence models, such as the *k*-*ε*, *k*-*ω* and SST models are evaluated by benchmarking their predictions against experimental data and those of the latest LES solvers. The main purpose of the study is to compare the performances of these models in simulating such a category of flows. In addition, the accuracy and factors that determine the success of such simulation are discussed. Our findings, for the first time, show that with a skillfully generated mesh and proper discretization schemes, the RANS approach with the above two-equation turbulence models are capable of capturing the salient features of the highly complex flow over the Ahmed body with a slant angle of 25°. The performances are as good as the LES solvers as reported in Serre *et al*. (2013), if not better for time-averaged flow simulations. The SST model produces the best results among the three models studied. This study could assist designers in the automotive industry in the applications of these cost-effective tools to improve their design productivity. Future study will focus on the performances of the models in simulating time-dependent flows over the Ahmed body.

KEY WORDS : Turbulence models, CFD, Ahmed body, LES, Automotive aerodynamics, Car aerodynamic design

NOMENCLATURE

ρ	: density, kg/m^3
u	: velocity, m/s
τ	: stress tensor, N/m^2
μ	: fluid dynamic viscosity, Pa·s
δ	: kronecker delta
x	: cartesian coordinates
k	: turbulence kenectic energy per unit mass, j/kg
ε	: turbulence dissipation rate per unit mass, j/(kg·s)
ω	: rate of dissipation of eddies, j/(kg·s)
v	: kinematic viscosity, m^2/s
Ω	: absolute value of vorticity, 1/s
C_D	: drag coefficient, dimentionless

SUBSCRIPTS

i, j	: cartesian coordinate indexes
t	: turbulence

**Corresponding author*: e-mail: yong.zhao@nu.edu.kz

1. INTRODUCTION

The automobile has become the most popular form of transport in many countries. However, fossil fuel consumption and emissions by automobiles have led to many diverse and long-term effects on the environment, which are of grave economic concerns. Numerous studies were implemented in order to improve the efficiency of the vehicles by reducing fuel consumption (Bhandarkar, 2013). It was claimed by Agarwal (2013) that reducing aerodynamic factors such as pressure drag and skin friction drag is more efficient and effective than engine modification and weight reduction of the automobile. Aerodynamic drag reduction can be achieved through geometry and flow modification of the vehicle. With this approach, fuel economy can be improved and other environmental issues such as noise and emissions will also be reduced (Banga *et al*., 2015).

Automotive aerodynamics is the study of air flow conditions, such as turbulent boundary layers and flow separation, wake development, viscous and pressure drags, aerodynamic noises, down forces and various causes of aerodynamic instability of road vehicles at high speeds. The steering and braking of the car can be better enhanced

by modifying the geometry and thus the air flow around the vehicle. Banga *et al*. (2015) estimated that more than half of the mechanical energy produced by the car is wasted through overcoming the aerodynamic drag at highway speed. According to Marklund (2013), the major portion of the drag is caused by the geometry of the car.

The balance of the lift and downward forces is another concern in automobile design. Downward forces are always desirable to maintain sufficient traction and cornering stabilities. However, increase in downward forces is the major cause of increase in the drag force which reduces the efficiency of the car due to increased fuel consumption. Thus, a balance of these two forces must be properly maintained for the vehicle for the purpose of minimum environmental impact (Banga *et al*., 2015).

The analysis of automotive aerodynamics can be conducted by both experiment and computer simulation. In recent decades, computational fluid dynamics (CFD) has matured to be a cost effective and efficient tool for aerodynamic analysis in the automotive industry (Barnard, 1996; Katz, 2016).

In this study, the Ahmed body is used as a benchmark for the analysis of car aerodynamics. This benchmark model was originally created by Ahmed *et al*. (1984), which is a bluff body with simple geometry for the study of the flow around it. The Ahmed body has a slanted rear end which allows the study of the effects of slant angles on flow characteristics to be investigated. Similar to typical flow over a car body, the flow over the Ahmed body can be highly complex, making the flow simulation extremely challenging. The Ahmed body was used in a benchmark test case for the ERCOFTAC/IAHR Workshops on Refined Flow Modelling (Jakirlic *et al*., 2001; Manceau and Bonnet 2002; Minguez *et al*., 2008; ERCOFTAC, 2017). It has become a useful test case in the development of efficient and accurate CFD tools for the evaluation of car designs.

Currently there are several approaches to simulating the flow over the car body and these include Reynolds-Averaged-Navier-Stokes (RANS) and Large-Eddy Simulation (LES) methods. The former uses time-averaging and turbulence models to calculate turbulent flows, while the latter uses fine meshes to directly resolve large turbulent eddies and model the small sub-grid-scale turbulence. The RANS method is much less computationally intensive and more widely used for industrial design and analysis than the LES. However, the RANS approach may not be capable of capturing highly complex turbulent flows compared with LES. Recently there have been a large amount of efforts in simulating the aerodynamic flow over the Ahmed body with various slant angles, using both the RANS (Han, 1989; Gilliéron and Chometon, 1999; Craft *et al*., 2001; Liu and Moser, 2003; Guilmineau, 2008; Kesarwani *et al*., 2014) and LES approaches (Hinterberger *et al*., 2004; Kapadia *et al*., 2004; Krajnovic and Davidson, 2005; Lehmkuhl *et al*., 2011; Serre, 2013).

According to Liu and Moser (2003), the RANS approach with a k-ε-$v2$ turbulence model is more accurate compared to the k-ε and full stress models for the wall-bounded case with separation. In their study, local flow conditions in different regions around the Ahmed body with a slant angle of 35^{o} were investigated. Their work indicated that the upwind differencing scheme is not as accurate as the second- order central differencing scheme. This study also compared the Reynolds Stress Model (RSM) and other two-equation models such as the k-ε turbulence model and suggested that the RSM model performed better than the k-ε one, but both could not be used for accurate prediction of the pressure drag. The study concluded that the RSM was not only useful in studying flows where streamline curvatures were significant, but also for flows over stagnation points and rotating flows. Numerous simulations have shown that the pressure variations over the front region of the Ahmed body would have the most significant effect on the behavior of drag (Kesarwani *et al*., 2014). Menter (1994) conducted an extensive review of the RANS approach with many two-equation turbulence models and concluded that this approach could successfully determine the flow over the Ahmed body with a 35^{o} slant angle. Nevertheless the approach could fail to generate satisfactory results for 25^{o} slant angle due to the separation and reattachment over the slant, which causes unsteady Kelvin-Helmholtz instability. As it is generally believed that the LES is more capable of simulating this kind of flow instability, this finding leads to extensive and detailed studies and comparisons of different LES solvers for the simulation of the flow over the Ahmed body with a 25^{o} slant angle. However, after a comprehensive study of various LES solvers and comparison of simulation results with experimental data, Serre *et al*. (2013) concluded that the Ahmed-body test case is still a challenge for all the latest LES solvers.

In this study, we carefully re-examine the RANS approach with three two-equation turbulence models to investigate if this approach is truly capable of simulating time-averaged flows over the Ahmed body with a 25^{o} slant angle. The aim is to determine and compare their predictive capabilities using the corresponding experimental data as benchmarks. The three turbulence models used are the standard k-ε, k-ω and SST (Shear Stress Transport) models. It is hoped that through this in-depth study, a solid conclusion can be reached regarding the capability of the RANS approach in tackling a class of automotive aerodynamics flows such as this one, when combined with a well generated mesh and suitable numerical schemes with appropriate turbulence models. This will enhance the confidence of car designers in using it for accurate and efficient analysis of automotive aerodynamics in future industrial applications.

2. GOVERNING EQUATIONS

The governing equations for steady state flow conditions are used to predict the flow around the Ahmed body. Computation is based on the Reynold-Averaged Navier-Stokes Equations (RANS), which include the continuity and momentum equations:

$$\frac{\partial}{\partial x_i}(\rho u_i) = 0 \tag{1}$$

$$\frac{\partial}{\partial x_j}(\rho u_i u_j) = \frac{\partial \rho}{\partial x_i} + \frac{\partial}{\partial x_j}(\tau_{ij} + \tau_{ij}^R) \tag{2}$$

$$\tau_{ij} = \mu\left(\frac{\partial u_i}{\partial x_j} + \frac{\partial u_j}{\partial x_i} - \frac{2}{3}\delta_{ij}\frac{\partial u_k}{\partial x_k}\right) \tag{3}$$

Equations (4) ~ (8) below are the transport equations for turbulent kinetic energy and its dissipation rate used for the two-equation turbulence models:

$$\frac{\partial}{\partial x_i}(\rho u_i k) = \frac{\partial}{\partial x_i}\left(\left(\mu + \frac{\mu_i}{\sigma_k}\right)\frac{\partial k}{\partial x_i}\right) + S_k \tag{4}$$

$$S_k = \tau_{ij}^R \frac{\partial u_i}{\partial x_j} - \rho\varepsilon + \mu_t P_B \tag{5}$$

$$\frac{\partial}{\partial x_i}(\rho u_i \varepsilon) = \frac{\partial}{\partial x_i}\left(\left(\mu + \frac{\mu_i}{\sigma_\varepsilon}\right)\frac{\partial \varepsilon}{\partial x_i}\right) + S_\varepsilon \tag{6}$$

$$S_\varepsilon = C_{\varepsilon 1}\frac{\varepsilon}{k}\left(f_1 \tau_{ij}^R \frac{\partial u_i}{\partial x_j} + \mu_t C_B P_B\right) - C_{\varepsilon 2} f_2 \frac{\rho\varepsilon^2}{k} \tag{7}$$

The Shear Stress Transport (SST) turbulence model consists of the well-known k-ω model near the wall and k-ε transport model in the free stream (Menter, 1994):

$$\frac{\partial(\rho k)}{\partial t} + \frac{\partial(\rho u_j k)}{\partial x_j} = \rho P - \beta^* \rho\omega k + \frac{\partial}{\partial x_j}\left((\mu + \sigma_k \mu_t)\frac{\partial k}{\partial x_j}\right) \tag{8}$$

$$\frac{\partial(\rho\omega)}{\partial t} + \frac{\partial(\rho u_j \omega)}{\partial x_j} = \frac{\gamma}{\nu_t} P - \beta\rho\omega^2 + \frac{\partial}{\partial x_j}\left((\mu + \sigma_\omega \mu_t)\frac{\partial \omega}{\partial x_j}\right) + 2(1 - F_1)\frac{\rho\sigma_{\omega 2}}{\omega}\frac{\partial k}{\partial x_j}\frac{\partial \omega}{\partial x_j} \tag{9}$$

where $P = \tau_{ij}\dfrac{\partial u_i}{\partial x_j}$

The constant ϕ of the new model are found using Equation (12) below:

$$\phi = F_1 \phi_1 + (1 - F_1)\phi_2 \tag{10}$$

Eddy viscosity is calculated with

$$\nu_t = \frac{\alpha_1 k}{\max(\alpha_1 \Omega; \Omega F_2)} \tag{11}$$

Where Ω is the absolute value of the vorticity and also:

$$F_1 = \tanh(ar\, g_1) \text{ and } F_2 = \tanh(ar\, g_2) \tag{12}$$

$$ar\, g_1 = \min\left[\max\left(\frac{\sqrt{k}}{0.09\omega y}; \frac{500\nu}{y^2\omega}\right), \frac{3.424\rho k}{CD_{k\omega} y^2}\right] \tag{13}$$

$$ar\, g_2 = \max\left(2\frac{\sqrt{k}}{0.09\omega y}; \frac{500\nu}{y^2\omega}\right) \tag{14}$$

$$CD_{k\omega} = \max\left(1.712\rho\frac{1}{\omega}\frac{\partial k}{\partial k_j}\frac{\partial \omega}{\partial x_j}, 10^{-20}\right) \tag{15}$$

For different turbulence closures, their model coefficients are as follows:

k-ω model: $\sigma_k = 0.6$; $\sigma_\omega = 0.5$; $\beta^* = 0.09$
k-ε model: $\sigma_k = 1.00$; $\sigma_\varepsilon = 0.856$
SST model: $\beta^* = 0.09$; $\alpha_1 = 0.31$; $\sigma_\omega = 0.5$; $\sigma_{\omega 2} = 0.856$

The wall function formulations for the standard k-ε model and the values of coefficients for all turbulence models used can be found in Ansys (2006).

3. NUMERICAL MODEL SETUP

The computer simulation is performed using the Ansys Fluent CFD package. The numerical model is established based on the experiment performed by Lienhart *et al.* (2002). The experiment was conducted in a low speed LSTM wind tunnel with ¾ open test section, such that the wind tunnel walls can be assumed to be far enough from the simulated body. The blockage ratio of 4 % was determined from the $A_{tunnel}/A_{frontal}$ ratio; and turbulence intensity for the experiment was less than 0.25 %. The CFD simulation considers only a half of the model due to geometric and flow symmetry under time-averaged conditions. Table 1 shows the parameters and conditions used in the simulation.

For the inlet velocity of 40 m/s at 25 °C, the air flow is considered as incompressible and the Mach number is less than 0.3.

3.1. Computational Domain

The dimensions and 3D model of the Ahmed body are given in Figures 1 (a) and (b). The dimensions of the computational domain shown in Figure 2 are as follows:

Table 1. Flow parameters.

Parameters	Value
μ_{air}	15×10^{-6} m^2/s
Material	Air, 25 °C
Reynolds number based on height of the body	768000
Inlet velocity	40 m/s
Outlet velocity	0 m/s
Height of car	288 mm
Car body, side plane, sky and ground	No slip walls
Symplane	Symmetry plane

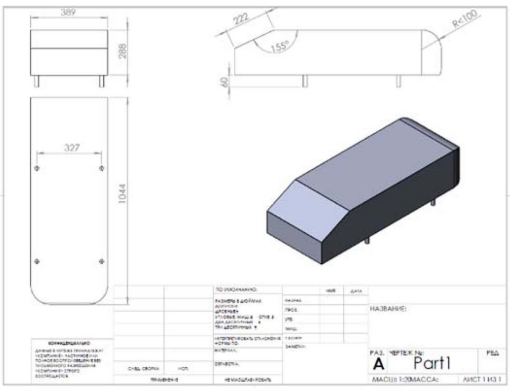

(a)

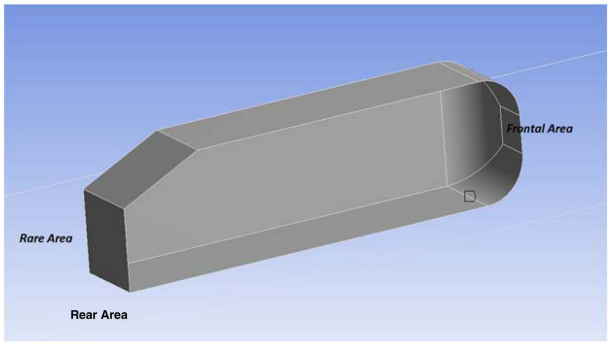

(b)

Figure 1. Ahmed body: (a) Its dimensions; (b) Its 3D model.

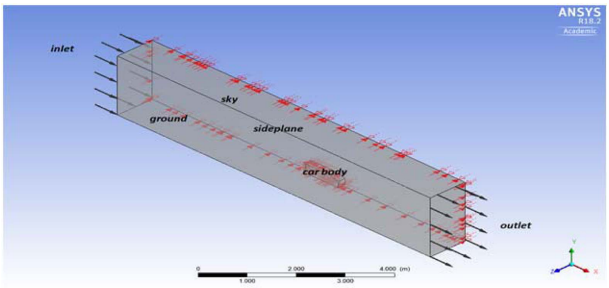

Figure 2. Computational domain.

W (z-axis) = 1000 mm
L (x-axis) = 9000 mm
H (y-axis) = 1870 mm

The distance from the inlet to frontal area is 4500 mm.

4. MESH CONVERGENCE STUDY AND MODEL VALIDATION

Apart from turbulence modeling, the discretization of the computational domain is a critical step for obtaining accurate results. Proper meshing should be ensured before one can investigate the accuracy of the turbulence models used. To improve computational efficiency without sacrificing accuracy, the meshes near the car body and on the other high gradients regions are refined. In particular exponentially expended structured mesh is used near the solid surfaces to accurately capture the turbulent boundary layers. A typical mesh generated for flow simulation is shown in Figures 3 (a) and elaborate structured mesh with exponential mesh expansion has been adopted for high resolution of the turbulent separated boundary layers (Figure 3 (b)). The discretization schemes used in this study are the QUICK and third-order MUSCL schemes for structured and unstructured meshes respectively for better resolution of the complex flow studied.

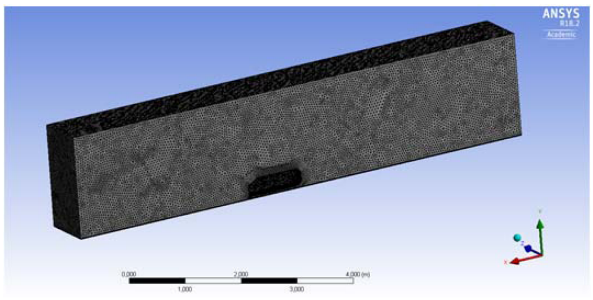

(a)

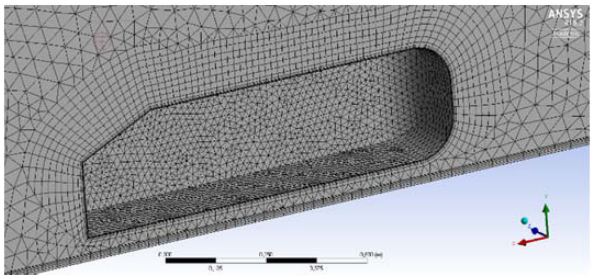

(b)

Figure 3. (a) Over view of a typical mesh used; (b) Zoom-in view of the structured mesh around the car body.

A mesh convergence study is conducted to ensure that the differences of monitored computational results are less than 1 % with progressively refined meshes. Three parameters were monitored: minimum velocity, drag and minimum pressure located 1.2 meters from the origin. The optimal mesh was found to mesh No. 4, which has 1,697,845 computational elements as shown in Tables 2 and 3. It should be noted here that the enhanced wall treatment option has been adopted. This combines a blended law-of-the wall and a two-layer zonal model for LRN turbulence models for flows with complex near-wall phenomena (Ansys, 2006), which makes the simulation less sensitive to the Y+ value being used.

For the validation, the experimental results from Lienhart *et al*. (2002) are used for comparison with the computed results of the SST, k-ε, k-ω turbulence models. Table 5 shows the computed and experimental velocities at the five probes, whose coordinate locations are indicated in

Table 2. Mesh convergence study.

Mesh #	Number of elements	Drag force (N)	Min velocity (m/s)	Min pressure (Pa)
1	461985	17.1007	23.1326	– 1481.24
2	747175	16.9947	23.7664	– 1481.68
3	1127547	16.2979	22.8134	– 1468.79
4	1697845	16.2180	23.0575	– 1454.39
5	1700018	16.1677	22.8408	– 1447.41
6	1703001	16.3108	22.0322	– 1473.11
7	1706575	15.8850	22.4144	– 1447.37
8	1711937	15.8694	22.9207	– 1453.02
9	1715981	15.8704	23.3705	– 1453.19
10	1721647	15.9369	23.7582	– 1456.67

Table 3. Errors of selected parameters during refinement of the mesh.

Mesh #	Error of drag (%)	Error of minvelocity (%)	Error of minpressure (%)	Max Y+
1				75.39
2	0.62	2.74	0.03	75.37
3	4.10	4.01	0.87	76.09
4	0.49	1.07	0.98	76.15
5	0.31	0.91	0.48	76.35
6	0.89	3.54	1.78	38.17
7	2.61	1.73	1.75	18.25
8	0.1	2.26	0.39	8.97
9	0.01	1.96	0.01	5.43
10	0.42	1.66	0.24	0.17

Table 4. Probe coordinates.

Probe #	X (mm)	Y (mm)	Z (mm)
1	80	338	100
2	80	28	100
3	500	178	160
4	1062	148	0
5	1442	28	0

Table 4. Velocity errors for different turbulence models are tabulated in Table 6.

The computed and experimentally measured drag coefficients are also compared in Tables 7 for the three

Table 5. Computed and experimental velocities at the five probes.

Probe #	SST (m/s)	k-ε (m/s)	k-ω (m/s)	Experimental data (m/s)
1	34.949	35.060	34.810	34.359
2	10.810	10.963	10.869	9.298
3	31.121	30.564	30.596	33.046
4	37.546	36.573	35.003	39.808
5	42.058	38.205	41.028	41.013

Table 6. Velocity errors for different turbulence models.

Probe #	SST (%)	k-ε (%)	k-ω (%)
1	1.719	2.040	1.313
2	16.259	17.904	16.896
3	5.824	7.511	7.413
4	5.682	8.127	12.071
5	2.547	6.849	0.036
RMS	**1.339**	1.992	2.130

Table 7. Computed drag coefficients C_D with different turbulence models and their comparisons with experimental measurement and their errors.

Turbulence models	Drag coefficient	Drag coefficient error (%)
SST	0.290	2.474
k-ε	0.320	13.074
k-ω	0.300	6.007
DES-SST (Serre *et al*., 2013)	0.343	15.101
LES-NWR (Serre *et al*., 2013)	0.346	16.107
LES-NWM (Serre *et al*., 2013)	0.317	6.376
LES-SVV (Serre *et al*., 2013)	0.431	44.631
Experimental Data (Ahmed *et al*., 1984)	0.298	NA

turbulence models as well as the LES models used by Serre *et al*. (2013). The comparison shows that the SST model surprisingly produces the best results among all the models investigated.

5. RESULTS AND DISCUSSION

Figure 4 (a) shows the pressure distribution around the car

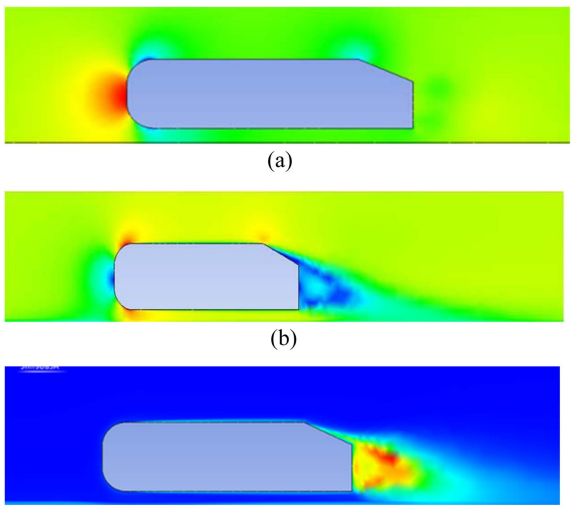

Figure 4. (a) Pressure contours around the car body; (b) Velocity magnitude contours; (c) Turbulence kinetic energy contours.

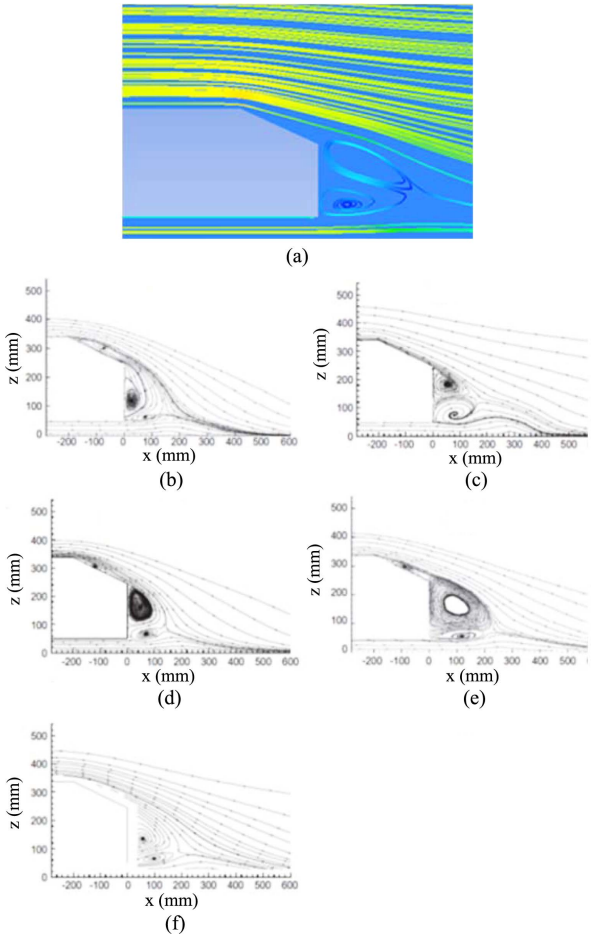

Figure 5. (a) Streamlines around the car body; (b) ~ (e) Streamlines predicted by LES solvers as reported in Serre *et al*. (2013); (f) Experimental measurement (Lienhart *et al*., 2002).

body as pressure contours by the SST model. In front of the car the pressure is highest, which corresponds to the stagnation point. The velocity magnitude contours are presented in Figure 4 (b). On the front of the car the velocity decreases close to the stagnation point, leading to the increment of the static pressure. Additionally, it can be seen around the corners that the velocity starts to increase due to favorable pressure gradients there. This leads to a drop in pressure. The predicted turbulence kinetic energy can be seen in Figure 4 (c), where it is mainly produced in the boundary layer over the slant and in the near wake region of the body.

Figure 5 illustrates the streamlines of the flow modeled by the SST turbulence model and the predictions by various LES solvers as reported in Serre *et al*. (2013) and the corresponding experimental measurement. Again the prediction by the two-equation turbulence model compares favorably with the experimental measurement, in comparison with those of the LES solvers.

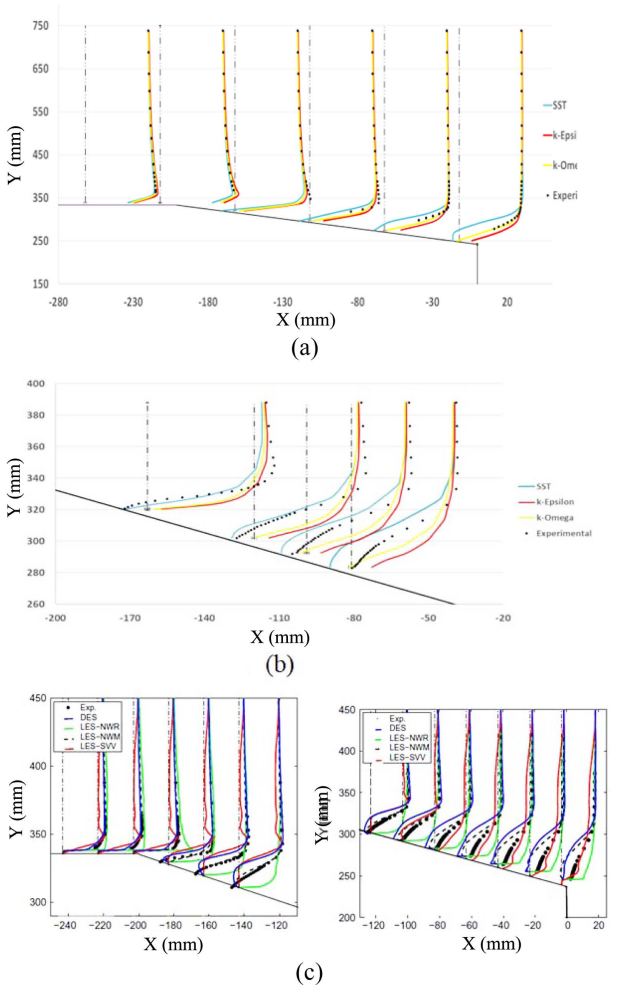

Figure 6. Velocity profiles over the slant of the Ahmed body and their comparisons with predictions by LES solvers reported in Serre *et al*. (2013) and experimental data (Lienhart *et al*., 2002).

Figure 6 shows the velocity profiles over the slant of the Ahmed body which are compared with the predictions by Large eddies simulations and experimental data. Figure 6 (a) shows selected velocity profiles over the whole slant predicted by the three turbulence models and their comparisons with the corresponding experimental data, while Figure 6 (b) gives more details of the predicted and measured velocity distributions near the wall in the middle of the slant. Generally speaking, the results obtained by the three turbulence models are found to agree with experimental measurements better than those of various LES codes in the region.

6. CONCLUSION

This paper investigates the RANS approach in details with three turbulence models for simulating the highly complex flow past the Ahmed car body with a slant angle of 25°. The results are compared with corresponding experimental findings and published results using LES. The simulated results by the RANS method with the three two-equation turbulence models show good correlation with experimental measurements, with the SST model producing the best results. With skillfully generated meshes and numerical schemes, they are in fact performing as good as many LES models, if not better for time-averaged flow conditions. It is hoped that the findings in this study could assist designers in the automotive industry in the applications of these cost-effective design tools to improve their design productivity. It is suggested that future study should focus on the performances of the models in simulating time-dependent flows over the Ahmed body.

ACKNOWLEDGEMENT–Any views pronounced or conclusions came to in this article are completely of the authors.

REFERENCES

Agarwal, R. K. (2013). Sustainable ground transportation – Review of technologies, challenges and opportunities. *Int. J. Energy and Environment (IJEE)* **4**, **6**, 1061–1078.

Ahmed, S. R., Ramm, G. and Faltin, G. (1984). Some salient features of the time-averaged ground vehicle wake. *SAE Paper No*. 840300.

Ansys (2006). Modeling Turbulent Flows: Introductory FLUENT Training. Ansys Inc.

Banga, S., Zunaid, M., Ansari, N. A., Sharma, S. and Dungriyal, R. S. (2015). CFD simulation of flow around external vehicle: Ahmed body. *IOSR J. Mechanical and Civil Engineering (IOSR-JMCE)* **12**, **4**, 87–94.

Barnard, B. H. (1996). *Road Vehicle Aerodynamic Design*. Longman. Harlow, UK.

Bhandarkar, S. (2013). Vehicular pollution, their effect on human health and mitigation measures. *Vehicle Engineering (VE)* **1**, **2**, 33–40.

Craft, T. J., Gant, S. E., Iacovides, H., Launder, B. E. and Robinson, C. M. E. (2001). Computational study of flow around the Ahmed car body (case 9.4). *Proc. 9th ERCOFTAC/IAHR Workshop on Refined Turbulence on Modelling*, Darmstadt, Germany.

ERCOFTAC (2017). "Classic Collection" Database. C. 82: Flow Around a Simplified Car Body, http://cfd.mace.manchester.ac.uk/cgi-bin/cfddb/prpage.cgi?82&EXP&database/cases/case82/Case_data&database/cases/case82&cas82_head.html&cas82_desc.html&cas82_meth.html&cas82_data.html&cas82_refs.html&cas82_rsol.html&1&0&0&0&0

Gilliéron, P. and Chometon, F. (1999). Modelling of stationary three-dimensional separated air flows around an Ahmed reference model. *ESAIM: Proc*., **7**, 173–182.

Guilmineau, E. (2008). Computational study of flow around a simplified car body. *J. Wind Engineering and Industrial Aerodynamics* **96**, **6-7**, 1207–1217.

Han, T. (1989). Computational analysis of three-dimensional turbulent flow around a bluff body in ground proximity. *AIAA J.* **27**, **9**, 1213–1219.

Hinterberger, C., Garcia-Villalba, M. and Rodi, W. (2004). Large eddy simulation of flow around the Ahmed body. *The Aerodynamics of Heavy Vehicles: Trucks, Buses, and Trains*, Berlin, Heidelberg, Germany, 77–87.

Jakirlic, S., Jester-Zucker, R. and Tropea, C. (2001). 9th ERCOFTAC/IAHR/COST Workshop on Refined Turbulence Modelling, Darmstadt, Germany.

Kapadia, S., Roy, S., Vallero, M., Wurtzler, K. and Forsythe, J. (2004). Detached-eddy simulation over a reference Ahmed car model. *Direct and Large-eddy Simulation V*, **9**, 481–488.

Katz, J. (2016). *Automotive Aerodynamics (Automotive Series)*. 1st edn. John Wiley & Son. Hoboken, New Jersey, USA.

Kesarwani, S., Jayas, Y. and Chhalotre, V. (2014). CFD analysis of flow processes around the reference ahmed vehicle model. *Int. J. Engineering Research & Technology* **3**, **3**, 775–780.

Krajnovic, S. and Davidson, L. (2005). Flow around a simplified car, Part 1: Large eddy simulation. *J. Fluids Engineering* **127**, **5**, 907–919.

Lehmkuhl, O., Borrel, R., P´erez-Segarra, C. D., Oliva, A. and Verstappen, R. (2011). LES modeling of the turbulent flow over an Ahmed car. *Direct and Large-Eddy Simulation VIII*, **15**, 89–94.

Lienhart, H., Stoots, C. and Becker, S. (2002). Flow and turbulence structures in the wake of a simplified car model (ahmed modell). *New Results in Numerical and Experimental Fluid Mechanics III*, **77**, 323–330.

Liu, Y. and Moser, A. (2003). Numerical modeling of air flow over the Ahmed body. *Proc. 11th Annual Conf. CFD Society of Canada*, Vancouver, Canada.

Manceau, R. and Bonnet, J. P. (2002). 10th Joint ERCOFTAC (SIG-15)/IAHR/QNET-CFD Workshop on Refined Turbulence Modelling, Poitiers, France.

Marklund, J. (2013). *Under-body and Diffuser Flows of Passenger Vehicles*. Chalmers University of Technology. Göteborg, Sweden.

Menter, F. R. (1994). Two-equation eddy-viscosity turbulence models for engineering applications. *AIAA J.* **32**, **8**, 1598–1605.

Minguez, M., Pasquetti, R. and Serre, E. (2008). High-order large-eddy simulation of flow over the "Ahmed body" car model. *Physics of Fluids* **20**, **9**, 95101.

Serre, E., Minguez, M., Pasquetti, R., Guilmineau, E., Deng, G. B., Kornhaas, M., Schäfer, M., Fröhlich, J., Hinterberger, C. and Rodi, W. (2013). On simulating the turbulent flow around the Ahmed body: A French–German collaborative evaluation of LES and DES. *Computers & Fluids*, **78**, 10–23.